Impact of austenite grain boundaries and ferrite nucleation on bainite formation in steels

Ravi, Ashwath M.; Kumar, Ankit; Herbig, Michael; Sietsma, Jilt; Santofimia, Maria J.

Important note
To cite this publication, please use the final published version (if applicable).
Please check the document version above.

Full length article

Impact of austenite grain boundaries and ferrite nucleation on bainite formation in steels

Ashwath M. Ravi[a,*], Ankit Kumar[a,b], Michael Herbig[b], Jilt Sietsma[a], Maria J. Santofimia[a]

[a] *Department of Materials Science and Engineering, Delft University of Technology, Mekelweg 2, Delft 2628 CD, the Netherlands*
[b] *Max-Planck-Institut für Eisenforschung GmbH, Max-Planck-Str. 1, Düsseldorf 40237, Germany*

A B S T R A C T

The rate of bainite formation depends on several factors such as austenite grain size, decomposition of austenite into other phases and austenite composition. Although studies have been carried out to understand various factors affecting bainite formation, open lines of investigation still remain. In this work, the effect of ferrite formation prior to bainite formation as well as the effect of parent austenite grain boundary composition on the bainite formation kinetics is investigated. With this aim, bainite formation treatments directly after complete austenitization and in combination with an intermediate heat treatment step prior to bainite formation were applied to a low-carbon silicon-containing steel. The intermediate heat treatment step leads to ferrite formation at and/or elemental segregation to austenite grain boundaries which were characterized using scanning electron microscopy, electron backscatter diffraction analysis and atom probe tomography. The results indicate that the kinetics of bainite formation can be accelerated with the help of an intermediate heat treatment step prior to bainite formation. The acceleration of bainite formation is mainly due to increase in the density of bainite nucleation sites.

1. Introduction

Bainitic microstructures form the crux of several modern steel grades [1–4]. However, despite the dominant presence of bainite in modern-day steels, several aspects of its formation are still unresolved [5–7]. Currently, bainite formation is one of the most intensely researched topics in steel metallurgy [1,5,8–16]. One of the major research topics is related to understanding the kinetics of bainite formation [17–22]. The isothermal bainite formation kinetics mainly depends on the composition of the steel and the temperature at which the bainite forms [17,19–21]. Additionally, the overall heat treatment which is applied prior to the bainite formation process influences the kinetics of bainite formation. For instance, parent austenite grain size, prior martensite formation and prior ferrite formation have all been shown to influence the rate of subsequent bainite formation [21–31]. Studies suggest that prior martensite formation can reduce the overall time required for subsequent bainite formation [22,27–29]. On the other hand, the effects of parent austenite grain size as well as prior ferrite formation on bainite kinetics are still under debate. With respect to the parent austenite grain size, some studies show that decreasing its size can accelerate the bainite

formation kinetics [1,23,24] while other studies show the contrary [25,26]. Such results have been related to the evolution of bainite microstructures within the austenite grain during the bainite formation [32]. Similarly, contradictory effects of prior ferrite formation on subsequent bainite formation kinetics have been reported in the literature. Quidort et al. argued that prior ferrite formation stimulates bainite formation [31] while Zhu et al. showed the opposite trend [30]. However, it must be pointed out that the studies regarding the effect of ferrite formation prior to bainite formation are very scarce in the literature. Such studies are nevertheless essential for efficient development of multi-phase microstructures where ferrite formation may precede bainite formation.

In addition to phase transformations prior to bainite formation, the austenite grain boundary condition, i.e., presence of interface precipitates or segregation of alloying elements to the austenite grain boundaries, affects the rate of bainite formation since austenite grain boundaries provide the potential nucleation sites for bainite formation [32]. Umemoto et al. [33] showed that precipitation of cementite or FeS at austenite grain boundaries can act as preferential nucleation sites and can lead to an acceleration of bainite kinetics. Furthermore, the elemental distribution of alloying elements in the vicinity of interfaces (such as austenite grain boundaries) will be determined in the prior heat treatments and can affect bainite formation. It should be noted that austenite grain boundaries are regions of defects in a material and solute segregation occurs to these interfaces [34]. The

heat treatment affects the transport of solute atoms to these interfaces, both thermodynamically and kinetically. The grain boundary segregation can influence the activation energy for bainite nucleation at austenite grain boundaries and consequently affect the rate of bainite formation. Nonetheless, little attention has been paid to understanding the influence of chemical composition in the vicinity of austenite grain boundaries on the rate of bainite formation in the literature.

In this work, a series of heat treatments is carried out to systematically investigate the influence of the overall heat treatment on the rate of bainite formation in a low-carbon silicon-containing steel. The effect of ferrite formation prior to bainite formation as well as the effect of chemical composition at and in the vicinity of austenite grain boundaries is the primary focus of this work. Isothermal bainite formation treatments are carried out directly after complete austenitization as well as following an intermediate annealing treatment at different temperatures for varying holding times. The intermediate annealing treatment employed prior to the bainite formation step is an isothermal heat treatment at a temperature between the austenitization temperature and the bainite formation temperature. The intermediate annealing treatment affects the austenite grain boundary condition via elemental segregation and/or austenite decomposition into ferrite near the austenite boundaries. It was observed that the kinetics of bainite formation can be influenced by the intermediate annealing treatment. These experiments provide insight into nucleation mechanism of bainitic ferrite at austenite boundaries. Furthermore, with the help of the results obtained from this work, the authors are able to propose strategies to control the kinetics of bainite formation.

2. Experiments

A hot rolled steel with a nominal composition of Fe−0.2C−3Mn−2Si (in wt%) was used in this study. 10 mm long cylindrical dilatometer samples with a diameter of 3.5 mm were machined from the hot-rolled plate. The samples were subjected to various heat treatments in a Bähr DIL805A/D dilatometer. The detailed time-temperature parameters used during various heat treatments are given in Fig. 1(a). Some samples were cooled to 400 °C for isothermal bainite formation directly after complete austenization, while other samples were subjected to an intermediate annealing treatment at different temperatures prior to the isothermal bainite treatment. The experimentally determined A_{c3} temperature of the steel used in this study is approximately 895 °C when a heating rate of 5 °C/s is employed.

In order to further understand the microstructural processes, the samples were subjected to a series of selected characterization techniques. Microstructural evolution during bainite formation was observed using optical microscopy and Scanning Electron Microscopy (SEM) techniques. Site-specific Atom Probe Tomography (APT) experiments were carried out to study the austenite grain boundary condition in terms of local chemical composition and nano-scale ferrite formation at the austenite grain boundaries prior to bainite

formation. An additional set of heat treatments was employed to produce samples for this APT study. Firstly, the as-received and machined dilatometer samples were homogenized at 1250 °C for 48 h to eliminate any artefacts related to chemical composition as a result macro-segregation of Mn in the steel. In order to ensure that the samples were not subjected to decarburization during homogenization, the samples were sealed within a quartz tube under argon atmosphere prior to the homogenization treatment. Following homogenization, the samples were heat treated according to the thermal profile given in Fig. 1(b), where some samples were subjected to an intermediate annealing treatment while others were cooled directly to 400 °C similar to the earlier heat treatments. It should be noted that the samples were immediately quenched at a rate of -400 °C/s from 400 °C. Considering such a high cooling rate, it can be assumed that the diffusion processes would not occur during cooling and the solute atoms would be frozen at their respective locations. Thus, the chemical composition observed at the austenite grain boundaries after these heat treatments will provide quantitative information regarding interfacial composition at the austenite grain boundaries prior to the start of the bainite formation at 400 °C.

It can be observed from the above experimental description that samples subjected to heat treatments given in Fig. 1(b) (i.e., samples used for APT) were homogenized while a such a homogenization treatment is not specified for samples subjected to heat treatments given in Fig. 1(a). The heat treatments described in Fig. 1(a) are used to study the effect of intermediate annealing treatment on bainite formation. For these studies, both homogenized and non-homogenized samples were used. However, obtained trends were similar regardless of homogenization. Thus, in order to clarify the effect of intermediate annealing treatment on bainite formation, results obtained with non-homogenized samples are used in this article since extensive amount data considering various intermediate annealing conditions was generated using non-homogenized samples compared to homogenized samples.

The site-specific studies were carried out following the steps described in already published works such as [35−37]. Electron Backscatter Diffraction (EBSD) analysis with a step size of 100 nm was carried out on the heat treated samples prepared for APT analysis to understand the crystallography of the microstructures obtained after different heat treatment conditions. EBSD data analysis was performed using TSL OIM software. ARPGE software [38] was employed to perform the prior austenite reconstruction using the EBSD data. With the help of the prior austenite reconstruction analysis, the sites for APT analysis in all samples, namely locations on a general high angle austenite grain boundary, were extracted. The misorientation angles of the isolated general high angle austenite grain boundaries lie within a narrow range of 40°−45° in order to ensure that results obtained from the APT measurements on different samples are comparable.

APT specimens were prepared from these isolated grain boundaries via Focused Ion Beam (FIB) milling according to the procedure described
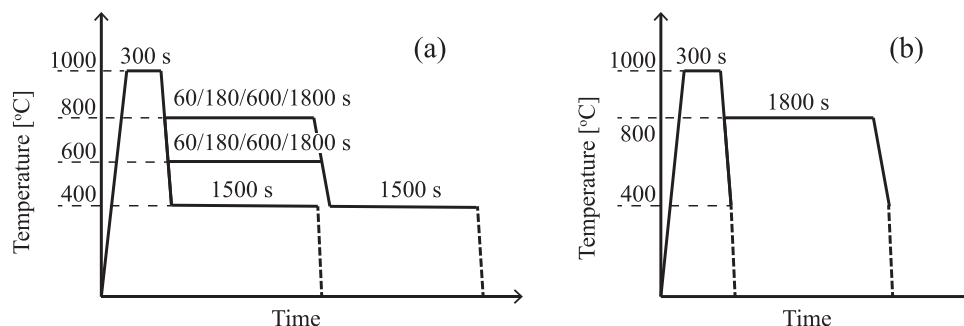

Fig. 1. (a) Schematic of heat treatment profiles used for understanding the effect of austenite grain boundary pre-conditioning on bainite formation kinetics. (b) Schematic of heat treatment profiles used prior to APT sample preparation. Heating was carried out at a rate of 5 °C/s while all the cooling steps prior to the isothermal bainite treatment were performed at -40 °C/s. After the bainite formation treatment, the samples were cooled to room temperature at a rate of almost -400 °C/s (dashed line).

in [39]. APT analyses were then performed using a Local Electrode Atom Probe (LEAP 3000 × HR, Cameca Instruments) in voltage mode at a specimen temperature of 65 K. During the APT experiments, the pulse fraction was 15% and the pulse frequency was 200 kHz. The data obtained from the APT experiments were reconstructed and analyzed using the IVAS software developed by Cameca Instruments. The reconstruction parameters were estimated using the technique described in [40].

3. Results

The experimental observations are illustrated in detail in the following sections.

3.1. Dilatometer results

Fig. 2 shows the kinetics of bainite formation at 400 °C in terms of change in length of the sample following complete austenitization and various additional intermediate annealing treatments. The degree of sample expansion corresponds with the volume fraction of bainite formed [32,41]. Bainite formation kinetics at 400 °C without any prior

intermediate annealing treatment is also plotted in Fig. 2 (solid lines in Fig. 2(a)–(d) indicated by intermediate annealing time equal to 0). Fig. 2(a) and (b) shows change in length of the sample as a function of time while Fig. 2(c) and (d) shows the corresponding rate of change in length of the dilatometer sample as a function of its linear expansion. Since the change in length of the sample is determined by the volume fraction of bainite formed, Fig. 2(c) and (d) essentially give the rate of bainite formation as the fraction of bainite increases. Fig. 2 shows that the annealing time and the annealing temperature used during the intermediate treatment play a role in the acceleration of the subsequent bainite formation. An increase in the intermediate annealing time and/ or a decrease in the intermediate annealing temperature increases the degree of acceleration of bainite formation.

Fig. 3 gives insight into the effect of intermediate annealing time-temperature parameters on the degree of acceleration of bainite formation kinetics. This degree of acceleration, Γ_{200}, is calculated as

$$\Gamma_{200} = \Delta L_{I200} / \Delta L_{O200} \tag{1}$$

ΔL_{I200} is the observed change in length of the sample after 200 s from the start of bainite formation treatment following a particular
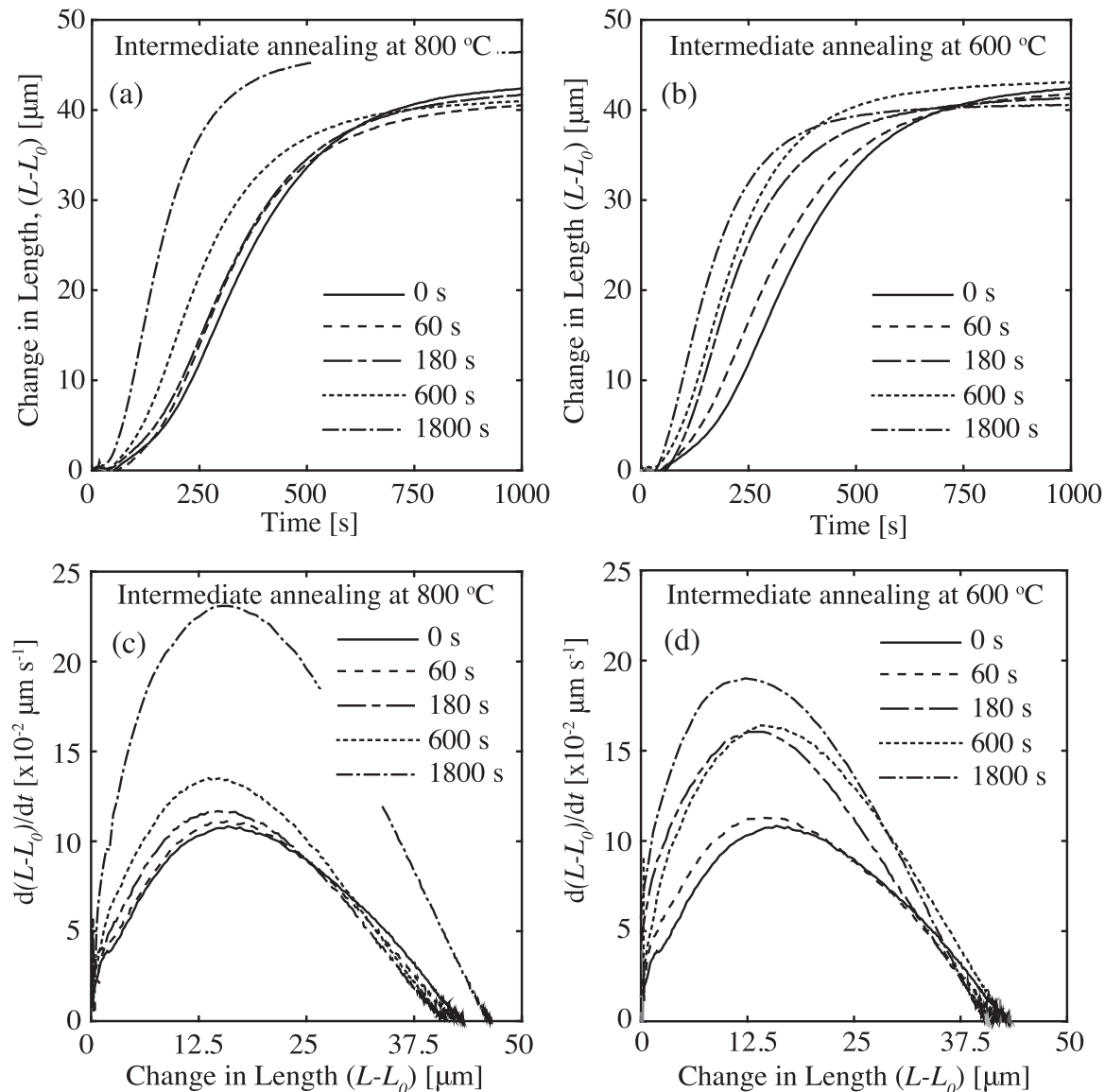

Fig. 2. Change in length of the sample during bainite formation treatment after intermediate annealing treatment (a) at 800 °C and (b) at 600 °C for varying holding times. Corresponding rate of change of length w.r.t sample length change after intermediate annealing treatment (c) at 800 °C and (d) at 600 °C for varying holding times. In all figures, holding time of 0 seconds represents bainite formation treatment without any intermediate annealing treatment (solid lines).
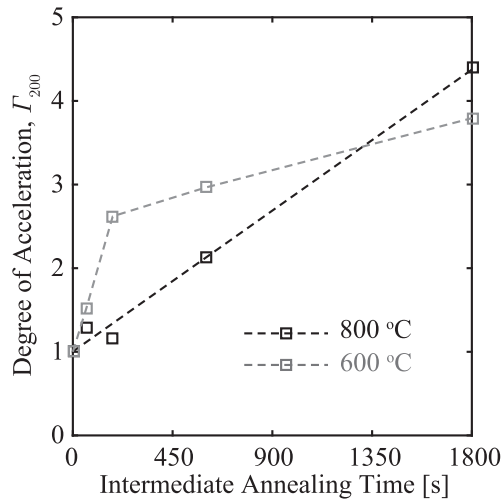
Fig. 3. Degree of acceleration, Γ_{200}, of bainite formation kinetics as a function of holding time during various intermediate annealing treatments.

intermediate annealing treatment and ΔL_{O200} is the corresponding change in length of the sample during bainite formation without intermediate annealing treatment. Γ_{200} is greater than 1 when the intermediate annealing treatment results in the acceleration of bainite formation kinetics. Fig. 3 shows that, within the range of the experiments performed, Γ_{200} increases linearly with increasing intermediate annealing time when the intermediate annealing temperature is 800 °C. In case of an intermediate annealing at 600 °C, Γ_{200} increases strongly when the intermediate annealing time is short. However, for longer annealing times, Γ_{200} increases at a lower rate. The possible reasons behind these trends are further discussed in Section 4.

Thermo-Calc calculations indicate that there is a chemical driving force for austenite to ferrite transformation below 812 °C, which implies that the intermediate annealing treatment can lead to ferrite formation. Fig. 4 shows the dilatometer results pertaining to the change in the length of the sample during intermediate annealing treatment at 800 °C and 600 °C. Similar to austenite to bainite transformation, ferrite formation leads to an expansion of the sample. Fig. 4 shows that dilatometry gives no indication of ferrite growth during intermediate annealing treatment at 800 °C, while ferrite formation is indicated to continuously occur during intermediate annealing treatment at 600 °C. Similar results are observed during microstructure analysis and APT experiments as shown in Sections 3.2 and 3.3, respectively. It should be noted that in Fig. 4, the change in
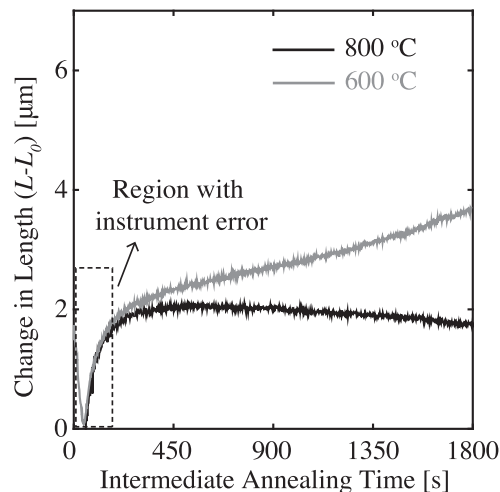
length of the sample observed within the first 200 s is related to an instrument error which is caused due to change in atmosphere within the dilatometer. The cooling step before the intermediate annealing treatment was carried out using a controlled flow of He gas while the isothermal annealing treatment was carried out in vacuum. The time required for the evacuation of the chamber during the intermediate annealing treatment following He injection during the previous cooling step led to the instrumental error seen during the initial 200 s of the intermediate annealing treatment. Fig. 4 shows that this change in length due to instrumental error is around 2 μm and is independent of annealing temperature. It can be postulated that this instrumental error occurs during bainite formation at 400 °C as well. However, Fig. 2 shows that the change in length at 400 °C is higher than 2 μm in all cases in the first 200 s of the bainite-formation treatment. Therefore, the recorded sample dilatation during the first 200 s could be attributed to both bainite formation and instrumental error. The instrumental error will influence the calculation of Γ_{200}. However, since this error is constant and independent of annealing temperature (Fig. 4), trend observed for Γ_{200} in Fig. 3 would not be affected.

3.2. Microstructural evolution

Fig. 5 sheds light on the microstructural evolution of bainite without and with intermediate annealing treatment. Fig. 5(a) shows a bainitic microstructure with martensite/austenite islands (formed during final quenching) which is obtained after a bainite treatment without any intermediate annealing. By comparing the microstructures shown in Fig. 5 to previously published results [1], it can be postulated that upper bainite forms during the isothermal treatment at 400 °C. Fig. 5(b) and (c) gives the microstructure obtained when bainite formation treatment was carried out after an intermediate annealing treatment at 600 °C and 800 °C for 10 min, showing that the obtained microstructures are almost identical in spite of the different heat treatment routes. Similar microstructure is obtained when bainite treatment is carried out after an intermediate annealing treatment at 800 °C for 30 min. Unlike these figures, Fig. 5(d) shows a mixed microstructure where both ferrite and bainite are present. This microstructure was obtained after bainite formation following an intermediate annealing treatment at 600 °C for 30 min. Based on the image analysis of the obtained optical micrographs, a maximum of 5% ferrite is formed during intermediate annealing treatment at 600 °C for 30 min. These results correspond well with the results presented in Section 3.1 where ferrite formation was observed by dilatometry only during the intermediate annealing treatment at 600 °C. Comparing the dilatometer results and the microstructural studies, it can be argued that when a holding time of less than 10 min is employed during intermediate annealing treatment at 600 °C, the fraction of ferrite formed may be too small to be detected via microscopy, while a holding time greater than 10 min leads to observable ferrite growth.

3.3. Site-specific APT studies

Since dilatometer and microstructural studies did not reveal any ferrite growth during intermediate treatment at 800 °C, site-specific APT studies were carried out as a higher resolution experiment to explore the reasons behind the accelerating effect of these treatments on subsequent bainite kinetics. APT studies can reveal any local chemical composition variation in the vicinity of parent austenite boundaries as well as any nano-scale ferrite growth during which carbon partitioning takes place as a result of intermediate annealing treatment.

In Fig. 6, the APT results based on the site-specific investigations carried out in the vicinity of parent austenite boundaries are compiled. Fig. 6(a)–(e) shows the results from samples which were directly quenched without any prior intermediate annealing
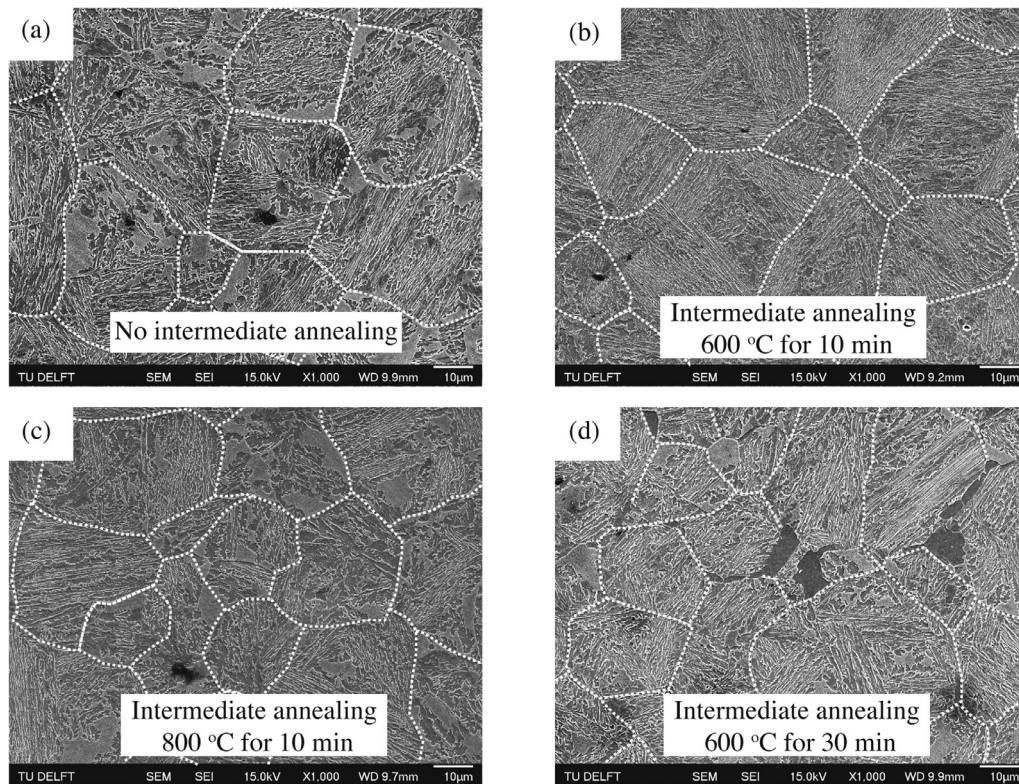

Fig. 4. Change in length of the sample during intermediate annealing treatment.

Fig. 5. Microstructures obtained after bainite treatment (a) without intermediate annealing treatment, (b) with intermediate annealing treatment at 600 °C for 10 min, (c) with intermediate annealing treatment at 800 °C for 10 min and (d) with intermediate annealing treatment at 600 °C for 30 min. Figures (a) - (d) are obtained via SEM analysis. In all figures, needle-shaped regions are bainite while lightly etched or unetched regions are martensite/austenite islands. Also, white dashed lines indicate prior austenite boundaries. In Figures (d), large dark etched islands denote ferrite formed during intermediate annealing treatment. The ferrite islands are observed in the vicinity of prior austenite boundaries.

treatment while Fig. 6(f)–(j) shows the results from samples which were quenched after a prior intermediate annealing treatment at 800 °C for 30 min. Fig. 6(a) and (f) gives the microstructure location from which the atom probe tips were lifted out for the APT study. In order to calculate the variation in local chemical composition at the interface, a cuboid shaped region of interest (ROI) with dimensions of 45 nm × 20 nm × 20 nm with the longest axis normal to the parent austenite boundary was chosen. The elemental distributions in and around the ROI are shown in Fig. 6(b) and (g). Based on the elemental distribution, Gibbs Interface Excess (GIE) plots were calculated within the ROI (Fig. 6(c)–(d) and (h)–(i)). GIE plots give the number of atoms of a given element as compared to the total number of atoms within the volume of the ROI along its longest axis [42]. The slope of the GIE plot represents the concentration of a given element along the length of the ROI. It is evident that the GIE plot would be linear if there is no difference in composition along the length of the ROI and the slope of the GIE plot will be a constant. A change in slope indicates a difference in elemental distribution along the ROI.

APT results show no signs of segregation of Mn and Si to the parent austenite grain boundaries prior to bainite formation irrespective of the use of intermediate annealing during the heat treatments. Unlike Mn and Si, Fig. 6(d) and (i) shows that carbon segregation to austenite boundaries prior to bainite formation does occur. Based on the APT results, the degree of carbon segregation to the austenite grain boundaries is observed to increase during an intermediate annealing treatment. Using the GIE plots, the interfacial carbon excess at the prior austenite grain boundaries after the intermediate annealing treatment at 800 °C for 30 min is measured to be 9.2 atoms per nm^2 while the interfacial carbon excess at the prior austenite boundaries without any intermediate annealing is 4.2 atoms per nm^2. The interfacial carbon excess was calculated using the procedure described in [42].

It is important to point out that further statistical data regarding such carbon segregation as a result of intermediate annealing

treatment would strengthen the argument, but could unfortunately not be achieved during this work. Moreover, Herbig et al. [43] noted that the crystallography of the grain boundaries has an effect on the degree of carbon segregation. Thus, it is important to confirm if the observed carbon segregation is a result of the character of grain boundaries or the intermediate annealing treatment. However, as pointed out in the experimental section, all the parent austenite boundaries used for site-specific APT analysis in this work are high angle grain boundaries and have a misorientation angle between 40° and 45°. Such a criterion for site selection for APT studies was adopted to alleviate the effects of the character of grain boundaries on carbon segregation.

APT studies do not reveal any ferrite growth along the parent austenite grain boundaries at 800 °C. It should be noted that the low solubility of carbon in ferrite would have been highlighted in the APT results if ferritic regions were present during APT studies. It can be seen in Fig. 6 that the carbon concentration on either side of parent austenite grain boundaries is about 0.92 at%, which is equal to the bulk carbon carbon concentration of the steel. This indicates the presence of martensite which is expected to form upon cooling without any bainite formation. (Fig. 6(e) and (j)). This is consistent with the previously presented dilatometer and microstructural results.

4. Discussion

Based on the results illustrated in the previous sections, in-depth inferences regarding the effect of overall heat treatment on rate of bainite formation is derived in this discussion.

4.1. Bainite formation kinetics

The results described in Section 3.1 clearly show that the use of an intermediate annealing treatment prior to isothermal bainite
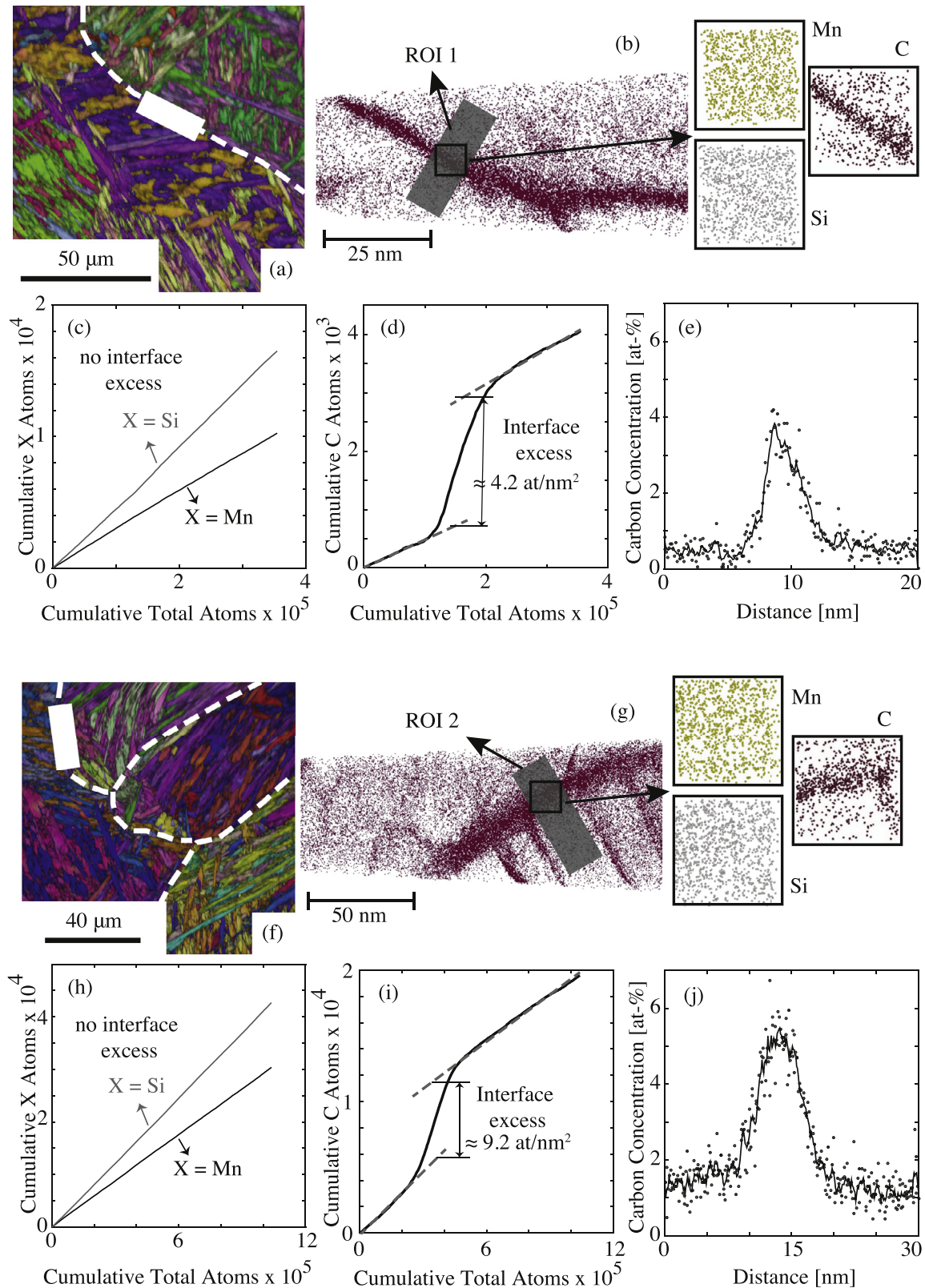
Fig. 6. APT results in samples which were directly quenched from 400 ℃ without any holding at this temperature. Figures (a)–(e) show the results in samples without any prior intermediate annealing treatment while Figures (f)–(j) show the results in samples with a prior intermediate annealing treatment at 800 ℃ for 30 min. (a) and (f) give the combined inverse pole figure and image quality map showing the prior austenite boundary (white dashed line) used for atom probe tips lift-out (white shaded rectangles). (b) and (g) give the reconstructed APT image showing overall C distribution along with atom maps of elements near the grain boundary regions (black squares). Grey shaded regions in the vicinity of the grain boundaries indicate the ROIs used to calculate the local compositional variations. (c) and (h) provide the ladder GIE plot of Mn and Si in ROI 1 and ROI 2 respectively whereas (d) and (i) show the ladder GIE plot of C in ROI 1 and ROI 2, respectively. (e) and (j) provide the carbon distribution across the grain boundary in ROI 1 and ROI 2 respectively. Dots shows the actual amount of carbon while the line shows the smoothed trend. The analysis for the ladder plot calculation and carbon distribution was carried out perpendicular to the respective grain boundary.

treatment leads to an acceleration of bainite formation kinetics. In order to understand these results better, the underlying rate determining factors are explored in this section. The influence of intermediate annealing treatment at 600 °C and 800 °C on these underlying factors is discussed in Sections 4.2 and 4.3.

The kinetics of bainite formation is dependent on the rate of bainite nucleation [17,44,45]. In a previously published paper [44], it was presented that the overall rate of bainite formation, df/dt, can be given in terms of rate of bainite nucleation at austenite grain boundaries and rate of autocatalytic bainite nucleation. It should be noted that bainite nucleation typically occurs at available interfaces and the rate of bainite nucleation depends on the type of the interface at which nucleation occurs [44]. With the approach given in [44], df/dt can be given as

$$\frac{df}{dt} = \kappa_p \left[\exp\left(\frac{-Q_G^*}{kT}\right) + \exp\left(\frac{-Q_A^*}{kT}\right) f \right] (1-f) \qquad (2)$$

where k is Boltzmann constant, T is the bainite formation temperature and f is the bainite fraction. Q_G^*, according to [44], gives the activation energy for bainite nucleation at austenite grain boundaries and Q_A^* is the activation energy for autocatalytic bainite nucleation at bainite/austenite interfaces. During bainite formation from a completely austenitic matrix, austenite grain boundaries are initially the only available interfaces. As bainite formation progresses, bainite/austenite interfaces are created and become available for further bainite formation. However, in the presence of an intermediate annealing treatment involving ferrite formation, bainite nucleation can occur at ferrite/austenite interfaces as well [31]. In such cases, Q_G^* is the effective activation energy for bainite nucleation at any previously existing interfaces of two different characters. The combination of austenite grain boundaries and ferrite/austenite interfaces is referred to as previously existing interfaces in this paper. κ_p is the pre-exponential factor and mainly accounts for the influence of the number density of initial nucleation sites, N, available at previously existing interfaces prior to bainite formation. According to [44], κ_p can be given as

$$\kappa_p \propto \frac{kT}{h} N \qquad (3)$$

where h is Planck constant. N depends on factors such as density of interfaces available and bainite formation temperature. Based on Eqs. (2) and (3), the rate of bainite formation under isothermal conditions depends on N, Q_G^* and Q_A^*.

Any influence of the intermediate annealing treatment on Q_A^* can be categorically ruled out due to two reasons. Firstly, Q_A^* affects the rate of bainite formation if bainite nucleation occurs at bainite/austenite interfaces. These interfaces are only created during the isothermal treatment at the isothermal bainite formation temperature and not during any prior treatment. Eq. (2) shows that Q_A^* is coupled with f which is 0 prior to the isothermal treatment at 400 °C. Secondly, the activation energy for bainite nucleation is dependent on the carbon concentration of austenite matrix in the vicinity of the interface at which the nucleation occurs [20,44]. APT results show that the intermediate annealing treatment at 800 °C only influences the carbon concentration at austenite grain boundaries while the carbon concentration within the bulk of the austenite remains practically unaffected. Additionally, microstructural results (Section 3.2) show that the maximum ferrite fraction formed during the intermediate annealing treatment at 600 °C is around 5%. Although ferrite formation is typically accompanied by carbon enrichment of surrounding austenite, such a low ferrite fraction will not influence the average carbon concentration of austenite significantly. Thus, it can be postulated that the carbon concentration of the austenite near the bainite/austenite interfaces, and consequently Q_A^*, would be similar regardless of the intermediate annealing treatment since the initial bulk composition of austenite grain is unaffected by it. This implies that

the experimentally observed acceleration of bainite formation kinetics is due to either a decrease in Q_G^* or an increase N, or both.

In order to understand the influence of Q_G^* and N on the rate of bainite formation, df/dt is computed for various Q_G^* and κ_p values using Eq. (2) (Fig. 7). It should be noted that since κ_p is directly proportional to N (Eq. 3), the effect of κ_p and N on df/dt would be similar. Q_A^* is assumed to be a constant (145 kJ/mol, based on results in literature [44,46]) in these calculations. This assumption does not affect the conclusions of this work since it does not play a role in accelerating bainite kinetics during the experiments carried out in this work. Using df/dt, the bainite evolution over time can be calculated (Fig. 7). In order to make a rigorous comparison between the experimentally determined data and the model calculations, the values for Q_G^* and κ_p are chosen such that the calculated time required for the completion of bainite formation is comparable with the corresponding experimentally observed value (Fig. 2).

Fig. 7(c) shows that the overall time required for bainite formation decreases as Q_G^* decreases. However, Q_G^* does not have any significant influence on the instantaneous rate of bainite formation as the bainite fraction increases (Fig. 7(d)). On the other hand, as κ_p (i.e., N) increases, the overall time required for bainite formation decreases (Fig. 7(a)) and the instantaneous rate of bainite formation increases (Fig. 7(b)). These trends can be explained by the mechanism of bainite formation. Since bainite formation begins at previously existing interfaces, a reduction in Q_G^* for a constant N implies that the bainite formation begins earlier in time. However, once the bainite formation begins, its formation rate is mainly controlled by nucleation at bainite/austenite interfaces where Q_G^* does not play a role. This is highlighted in Fig. 7(c) and (d). Unlike Q_G^*, N influences the rate of bainite nucleation at bainite/austenite interfaces as well as at austenite grain boundaries and ferrite/austenite interfaces. The above discussion suggests that the nucleation at previously existing interfaces is a precursor for autocatalytic nucleation at bainite/austenite interfaces. Thus, an increase in N results in the increase of the rate of autocatalytic nucleation as the density of autocatalytic nucleation sites increases. Since N influences both the rate of bainite formation at previous existing interfaces and at bainite/austenite interfaces, κ_p affects the instantaneous rate of bainite formation and the overall time required for bainite formation (Fig. 7(a) and (b)).

Fig. 7 can be compared with experimental results observed in Fig. 2. Experimental results show that the intermediate annealing treatment has an effect on both the overall time required for bainite formation and the instantaneous rate of bainite formation as a function of bainite fraction. This implies that the acceleration of bainite formation kinetics as a result of the applied intermediate annealing treatment is mainly due to the increase in N.

4.2. Effect of ferrite growth on bainite kinetics

As observed in Section 3, the intermediate annealing treatments at 600 °C can lead to observable ferrite growth while ferrite growth is undetected in other cases. Furthermore, results in Section 3.1 clearly show that the rate of bainite formation is influenced to a certain degree by the prior intermediate annealing treatment regardless of observable ferrite growth. In this section, bainite formation following intermediate annealing treatments which lead to observable ferrite growth is discussed. Additionally, the effect of intermediate annealing treatments on ferrite growth itself is also explored in this section. In Section 4.3, bainite formation following intermediate annealing treatments which do not lead to observable ferrite growth is discussed.

The results shown in earlier sections show that ferrite growth is detected only during intermediate annealing treatment at 600 °C with annealing times longer than 10 min. Thermo-calc calculations for the steel composition used in this study suggest that there is a driving force for ferrite formation below 812 °C. However, it must be realized that, although ferrite formation may be thermodynamically feasible, kinetic constraints need to be overcome for ferrite growth to
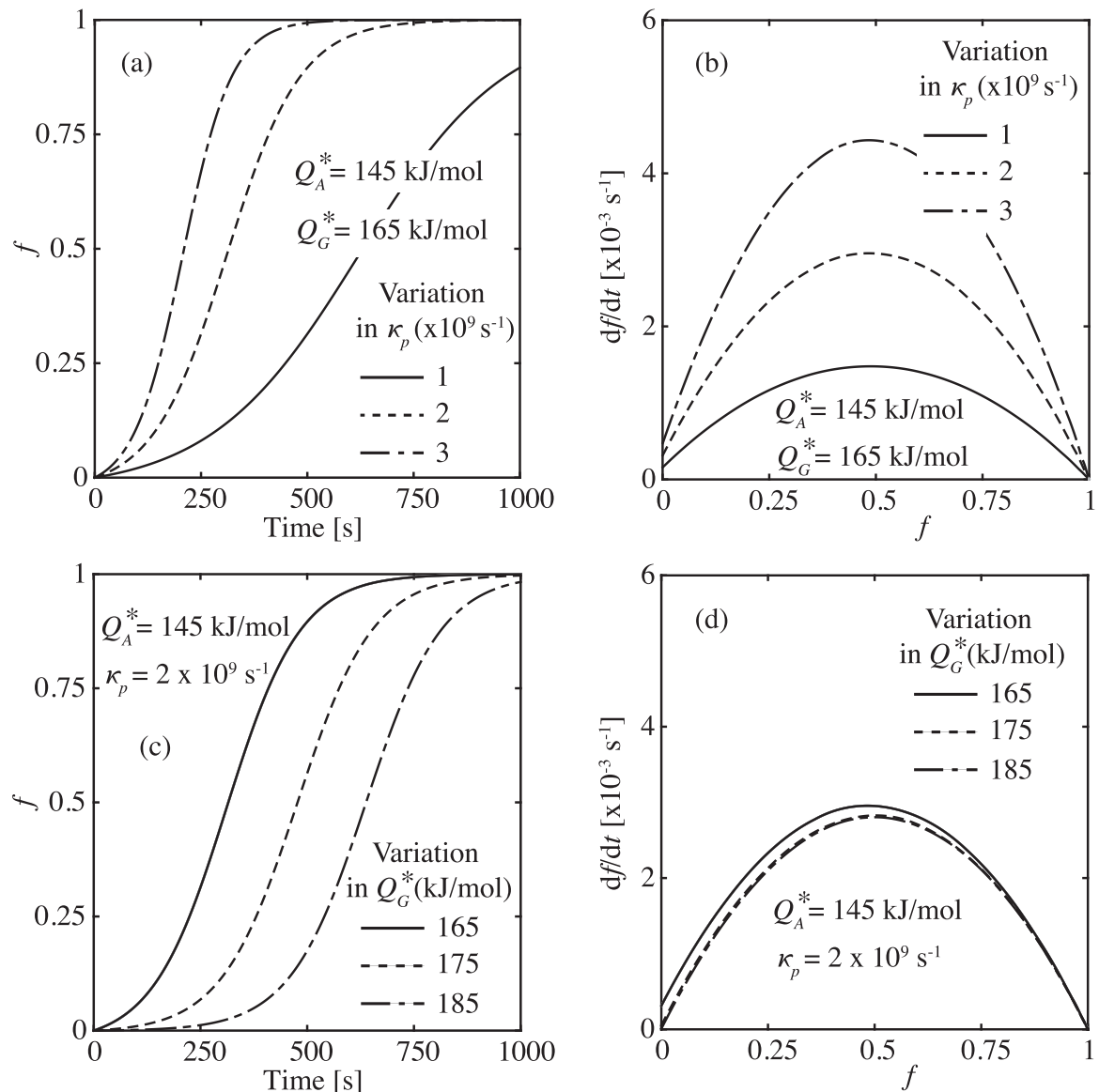
Fig. 7. Bainite evolution at 400 °C as a function of time with variation in (a) κ_p and (c) Q_G^*. Corresponding df/dt values as a function of bainite fraction, f with variation in (b) κ_p (d) Q_G^*. Increase in κ_p implies an increase in the number density of bainite nucleation sites.

occur. Literature reports suggest that the mode of the austenite to ferrite phase growth is controlled by the prevailing thermodynamic conditions, diffusivities of the alloying elements and interface mobility [47,48]. In general, the austenite to ferrite growth may occur in different ways – (i) with complete redistribution of alloying elements and the austenite and ferrite fraction in full equilibrium (ortho-equilibrium) (ii) with partitioning of substitutional alloying elements (or elements which diffuse slowly) between austenite and ferrite, and the interface in full local equilibrium condition (*Partitioning Local Equilibrium*, PLE); (iii) with negligible partitioning of substitutional alloying elements between austenite and ferrite, and the interface in full local equilibrium condition (*Negligible Partitioning Local Equilibrium*, NPLE) and (iv) without any redistribution of substitutional alloying elements (para-equilibrium) [47]. In all cases, carbon is assumed to partition between ferrite and austenite.

The mode of austenite to ferrite growth can be estimated using the equilibrium phase diagram. Fig. 8 shows the isothermal section (at 600 °C and 800 °C) through the Fe−C−Mn-2 wt% Si phase diagram with NPLE/PLE transition line. It can be seen in Fig. 8 that for the composition of the steel used in this study, the austenite to ferrite growth at 600 °C occurs under NPLE conditions while ferrite growth at 800 °C

occurs at PLE conditions. Typically, PLE conditions for ferrite growth are characterized by sluggish kinetics due to redistribution of substitutional alloying elements during ferrite growth, while under NPLE conditions ferrite growth is considerably faster. Moreover, it can be expected that ferrite nucleation rate at 800 °C is lower compared to at 600 °C due to the lower driving force for nucleation. These kinetic restrictions can explain the differences in the fraction of ferrite observed during the intermediate annealing treatment.

In Section 4.1, it was derived that the acceleration of bainite formation after an intermediate annealing treatment was due to an increase in number density of initial bainite nucleation sites, *N*. Ferrite growth prior to bainite treatment has a direct influence on the density of interfaces (consequently, *N*) available for bainite formation. Ferrite growth leads to the creation of ferrite/austenite interfaces. This implies that additional interfaces within the prior austenite grains are created and the total density of interfaces available for bainite nucleation increases.

Zhu et al. reported that the presence of ferrite/austenite interfaces retards the kinetics of subsequent bainite formation since the driving force for bainite nucleation at these interfaces is lower than the driving force for bainite nucleation at prior austenite grain boundaries
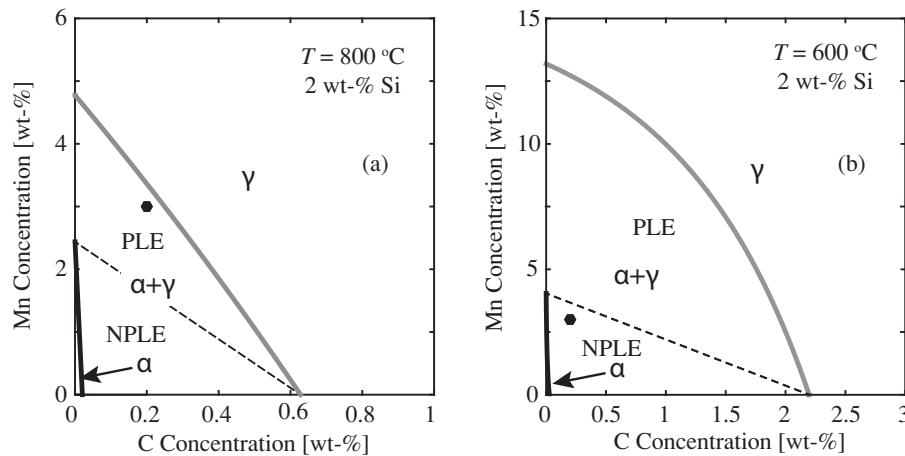
Fig. 8. Isothermal section through the Fe−C−Mn−2Si phase diagram (a) at 800 °C and (b) at 600 °C. The thick grey line shows the $\gamma/(\alpha+\gamma)$ phase boundary and the thick black line (close to y-axis) shows the $\alpha/(\alpha+\gamma)$ phase boundary. The dashed line shows the NPLE/PLE transition in the dual-phase $\alpha+\gamma$ region. The dot gives the composition of the steel used in this study.

[30]. Such a retarding effect is mainly due to partitioning of carbon into austenite during ferrite growth. Zhu et al. suggested that the partitioning of alloying elements leads to higher elemental (mainly C and Mn) concentration near the ferrite/austenite interfaces. It is evident that the partitioning of carbon into austenite during ferrite formation increases the chemical stability of austenite and thus, the driving force for subsequent bainite formation following ferrite formation during intermediate annealing treatment will be lower. However, the impact of carbon partitioning on the reduction of the driving force for bainite formation is not significant when the ferrite fraction is small [30], as is in the case for the experiments in this work. Quidort and Bréchet [31] postulated that the formation of around 10% of grain boundary ferrite can stimulate subsequent bainite formation.

4.3. Carbon segregation and its effect on bainite nucleation sites

During the intermediate annealing treatment at 800 °C as well as at 600 °C for annealing times less than 10 min, experimental results do not show any ferrite growth. However, this cannot be unequivocally claimed as complete absence of ferrite formation during these intermediate annealing treatments, especially since austenite transformation to ferrite is thermodynamically possible at these temperatures. But, based on the experimental results, it can be suggested that if ferrite formation does occur during these annealing treatments, the ferrite grains would be nano-scale in size and they would be sparsely dispersed along the parent austenite grain boundaries. Ferrite grains larger than 100 nm would have been detected during SEM/EBSD analysis. Additionally, if the ferrite grains were not sparsely dispersed, they would have been detected during APT analysis as low carbon regions near parent austenite grain boundaries due to low solubility of carbon in ferrite. Such small and sparsely dispersed ferrite grains will not have any considerable impact on the total density of interfaces. Thus, it can be argued that the acceleration of bainite formation kinetics in the presence of intermediate annealing treatment at 800 °C as well as during intermediate annealing treatment at 600 °C for shorter annealing times is not due to creation of ferrite/austenite interfaces, unlike as seen in Section 4.2. Under these circumstances, acceleration of bainite formation alludes to a different mechanism in play. This fits well with results given in Fig. 3 which shows that the rate of acceleration of bainite formation, Γ_{200}, changes when significant ferrite growth is observed during longer prior intermediate annealing treatment at 600 °C.

APT results presented in Section 3.3 show that the carbon segregation to austenite grain boundaries is more pronounced when an intermediate annealing treatment is used prior to bainite formation compared to when bainite formation occurs without any intermediate annealing. These results are in line with previously published experimental results [49–51]. Abe et al. carried out a two-step heat treatment in order to understand the segregation behavior of carbon and phosphorus in medium carbon steels [49]. In their study [49], samples were austenized at 1100 °C, followed by isothermal holding at temperatures between 800 °C and 1000 °C for 10−1000 s. The samples were then cooled to room temperature. Such a treatment is similar to the austenization and intermediate annealing treatment (Fig. 1(b)) used in this study. Abe et al. also observed that the use of a step treatment (or intermediate annealing treatment) led to increased carbon segregation at the austenite grain boundaries compared to samples directly cooled from the austenitization temperature (which would be the starting condition for bainite formation without intermediate annealing treatment) [49]. These results compare well with results presented in this work. In addition, Abe et al. suggested that the degree of carbon segregation during the intermediate annealing treatment increases with increasing holding time as well as with decreasing intermediate annealing temperature [49]. The role of such a increased carbon segregation to austenite grain boundaries as a result of intermediate annealing treatment in accelerating subsequent bainite formation kinetics can be explained using the discussion below.

Several previously published studies have hypothesized that solute segregation to grain boundaries during isothermal holding can lead to solute-rich and solute-poor areas within the austenite matrix [50–53]. Kang et al. studied the distribution of carbon in the vicinity of the austenite grain boundaries after short isothermal holding at 300 °C in several high carbon steels [50]. They observed that the isothermal holding led to carbon enrichment of the austenite grain boundaries as well as to the creation of carbon-depleted zones in near vicinity of the austenite grain boundary (upto a distance of 200 nm from the grain boundary) [50]. In a separate study, Zhang et al. reported similar results [51]. These results are in good agreement with the APT results presented in this work which show that intermediate annealing treatment (which is a isothermal holding step at an elevated temperature) leads to carbon segregation in the vicinity of austenite grain boundaries. Furthermore, comparing the published results in [50,51] with the APT results observed in this study, it can be postulated that the increased carbon segregation during intermediate annealing treatment would consequently lead to similar carbon-rich and carbon-poor areas. Kang et al. suggest that the formation of carbon-rich and carbon-poor areas during isothermal holding is a result of stress fields associated with the dislocations and grain boundaries [50]. Kang et al. argue that clustering of carbon atoms

occurs within the tensile zones near the dislocations and grain boundaries and carbon depletion occurs in the regions under compressive stress during isothermal holding [50]. The formation of carbon-rich and carbon-poor areas is referred to as a pre-bainitic phenomenon by Kang et al.. Furthermore, it is suggested that the low-carbon regions assist in the bainite nucleation process since the driving force for bainite formation increases with decrease in the carbon concentration of the austenite matrix. However, Bhadeshia argues that the formation carbon-depleted regions does not affect the kinetics of bainite formation since an equal fraction of carbon-rich regions would be created in the process which would counter-balance the effects of carbon-poor areas [1]. The longevity and thickness of carbon-depleted regions observed has also been questioned by certain researchers [53,54]. As mentioned previously, carbon segregation to austenite grain boundaries reduces their interfacial free energy [34]. Aaronson et al. argue that carbon-depleted regions in the immediate vicinity of austenite grain boundaries would exist only for a limited time until the chemical potential of carbon in the austenite grain boundary is the same as in the bulk [53]. Using the McLean model for kinetics of solute segregation [55], Umemoto et al. estimate that the carbon segregation to austenite grain boundaries should be practically instantaneous due to the high diffusion rate of carbon and near equilibrium segregation is expected to be achieved even during quenching [23]. Therefore in order to explain results seen by Kang et al. [50], Aaronson and Hirth [53] suggest that presence of extensively carbon-enriched regions and corresponding depleted regions during isothermal holding is indicative of austenite decomposition into phases with low carbon solubility, for instance ferrite.

The above hypothesis from Aaronson and Hirth [53] fits the experimental results observed in this study and forms the basis for the theory explaining the accelerated bainite kinetics as a result of intermediate annealing treatment. It can be argued that carbon segregation to austenite grain boundaries leads to fluctuations in carbon composition in its vicinity. These carbon fluctuations can result in the formation of stable ferrite nuclei during the intermediate annealing treatment especially since there is a driving force for ferrite formation at the annealing temperatures used in this study. However, kinetic constraints as seen in Section 4.2 will restrict the diffusional growth of these ferrite grains. If the intermediate annealing treatment already leads to body-centered cubic (BCC) ferrite nuclei with low carbon content in the vicinity of the austenite grain boundaries which grow into bainite once the isothermal bainite formation temperature is reached, the initiation time for bainite formation is reduced. This leads to acceleration of bainite kinetics. It can be argued that, during intermediate annealing treatment, the number of BCC ferrite nuclei increases with increasing annealing time and with decreasing annealing temperature (since chemical driving force for austenite to ferrite transformation increases). The above discussion explains the results observed in Fig. 3, which shows that the rate of bainite formation increases with increasing annealing time in the presence of an intermediate annealing treatment at 800 °C where no austenite to ferrite formation is detected. Additionally, the rate of bainite formation increases at a much higher rate in the presence of an intermediate annealing treatment at 600 °C when short annealing times are used. However, during longer annealing times at 600 °C, the BCC nuclei would grow to form ferrite rendering the nuclei formed during the intermediate annealing treatment unavailable for subsequent bainite formation. Under such circumstances, the rate of bainite formation is controlled by the increase in total density of interfaces as a result of formation of ferrite/austenite interfaces. It should be further pointed out that an increase in the number of BCC ferrite nuclei directly increases N which was determined as the primary rate controlling factor in Section 4.1.

During the experiments carried out in this work, the carbon-poor areas were not detected. However, it must be pointed out that these are difficult to detect via APT measurements since fast cooling to room temperature after intermediate annealing treatment leads to martensite formation in the low carbon steel used in this study. This leads to additional

interfaces and defects into which carbon segregation can further occur. Additionally, if ferrite nuclei form during the intermediate annealing treatment, their location would be difficult to isolate. It must be noted that, due to the composition of the steels in the studies of Kang et al. [50] and Zhang and Kelly [51], the room temperature microstructure obtained after a short isothermal holding at an elevated temperature and quenching is entirely austenitic. However, in the present study the carbon-rich areas along the austenite grain boundaries due to carbon segregation are immediately visible (Fig. 6) which can be extrapolated as indirect evidence for the fluctuation of carbon composition in the vicinity of austenite grain boundaries (bainitic nucleation sites) during intermediate annealing treatment.

Based on the evidence presented here, it can be postulated that carbon segregation during intermediate annealing treatment plays a role in the rate of subsequent bainite formation. Typically, without any intermediate annealing treatment, carbon segregation would occur at the bainite formation temperature. An intermediate annealing treatment assists to start the primary stages of bainite nucleation, and thus reducing the time required for overall bainite formation during subsequent treatment.

5. Conclusions

The effect of different heat treatment routes on the rate of bainite formation has been studied in this work with the help of a customized set of heat treatments. The results of this work show that the rate of bainite formation in low-carbon steels can be accelerated mainly via two mechanisms.

A small fraction of ferrite (less than 5%) formed prior to bainite formation increases the number density of interfaces available for bainite nucleation and consequently, leads to an increase in the rate of bainite formation. It is important to note that the rate of bainite formation increases only as long as the nucleation rate increases which is when the fraction of ferrite formed prior to bainite formation is small. As the fraction of ferrite formed increases, the activation energy for subsequent bainite formation increases and this, in extreme cases, can slow down the kinetics of the bainite formation. Furthermore, a short isothermal holding between the bainite formation and austenitization temperatures leads to increased carbon segregation to austenite grain boundaries prior to the start of bainite formation as compared to bainite formation without such treatment. The increased carbon segregation plays an important role in the acceleration of bainite kinetics as well.

Based on the results obtained, it can be further hypothesized that the rate of bainite formation can be manipulated by controlling the overall heat treatment route. In this study, intermediate annealing treatments are used for acceleration of bainite formation. Another energy-efficient route for introducing secondary nucleation sites is via appropriately choosing the austenitization temperature or a proper cooling rate. For instance, an austenitization temperature just below the A_{c3} temperature would create both the primary nucleation sites (austenite/austenite interfaces) and the secondary interfaces (austenite/ferrite interfaces) in the same heat treatment step. Such an austenitization temperature would automatically lead to an almost fully austenitic matrix with a minute fraction of ferrite at the interfaces. The small fraction of ferrite nestled within the austenite matrix would not affect the chemical composition of the austenite matrix for subsequent bainite formation. Furthermore, a tailored cooling rate can influence the carbon segregation at austenite grain boundaries as well as austenite decomposition into ferrite.

Declaration of Competing Interest

The authors declare that they have no known competing financial interests or personal relationships that could have appeared to influence the work reported in this paper.

Acknowledgments

References

[1] H.K.D.H. Bhadeshia, Bainite in Steels: Theory and Practice, third ed., Maney Publishing, 2015.

[2] F.G. Caballero, H.K.D.H. Bhadeshia, Very strong bainite, Curr. Opin. Solid State Mater. Sci. 8 (3−4) (2004) 251–257, doi: 10.1016/j.cossms.2004.09.005.

[3] H.K.D.H. Bhadeshia, Nanostructured bainite, Proc. R. Soc. Lond. A Math. Phys. Eng. Sci. 466 (2113) (2009) 3–18, doi: 10.1098/rspa.2009.0407.

[4] B.D. Cooman, Structure-properties relationship in TRIP steels containing carbide-free bainite, Curr. Opin. Solid State Mater. Sci. 8 (3−4) (2004) 285–303, doi: 10.1016/j.cossms.2004.10.002.

[5] L.C.D. Fielding, The bainite controversy, Mater. Sci. Technol. 29 (4) (2013) 383–399, doi: 10.1179/1743284712Y.0000000157.

[6] R.F. Hehemann, K.R. Kinsman, H.I. Aaronson, A debate on the bainite reaction, Metall. Trans. 3 (5) (1972) 1077–1094, doi: 10.1007/BF02642439.

[7] M. Hillert, The nature of bainite, ISIJ Int. 35 (9) (1995) 1134–1140, doi: 10.2355/isijinternational.35.1134.

[8] H.K.D.H. Bhadeshia, D.V. Edmonds, The mechanism of bainite formation in steels, Acta Metall. 28 (9) (1980) 1265–1273, doi: 10.1016/0001-6160(80)90082-6.

[9] W.T. Reynolds Jr., H.I. Aaronson, G. Spanos, A summary of the present diffusionist views on bainite, Mater. Trans. JIM 32 (8) (1991) 737–746, doi: 10.2320/matertrans1989.32.737.

[10] Z.-G. Yang, H.-S. Fang, An overview on bainite formation in steels, Curr. Opin. Solid State Mater. Sci. 9 (6) (2005) 277–286, doi: 10.1016/j.cossms.2006.06.005.

[11] F. Caballero, M. Miller, C. Garcia-Mateo, J. Cornide, New experimental evidence of the diffusionless transformation nature of bainite, J. Alloys Compd. 577 (2013) S626–S630, doi: 10.1016/j.jallcom.2012.02.130.Supplement 1

[12] H. Chen, S. van der Zwaag, A general mixed-mode model for the austenite-to-ferrite transformation kinetics in Fe−C−M alloys, Acta Mater. 72 (2014) 1–12, doi: 10.1016/j.actamat.2014.03.034.

[13] K. Rakha, H. Beladi, I. Timokhina, X. Xiong, S. Kabra, K.-D. Liss, P. Hodgson, On low temperature bainite transformation characteristics using in-situ neutron diffraction and atom probe tomography, Mater. Sci. Eng. A 589 (2014) 303–309, doi: 10.1016/j.msea.2013.09.055.

[14] I.B. Timokhina, K.D. Liss, D. Raabe, K. Rakha, H. Beladi, X.Y. Xiong, P.D. Hodgson, Growth of bainitic ferrite and carbon partitioning during the early stages of bainite transformation in a 2mass studied by in situ neutron diffraction, TEM and APT, J. Appl. Crystallogr. 49 (2) (2016) 399–414, doi: 10.1107/S1600576716000418.

[15] A. Kumar, A. Dutta, S. Makineni, M. Herbig, R. Petrov, J. Sietsma, In-situ observation of strain partitioning and damage development in continuously cooled carbide-free bainitic steels using micro digital image correlation, Mater. Sci. Eng. A 757 (2019) 107–116, doi: 10.1016/j.msea.2019.04.098.

[16] A. Kumar, S. Makineni, A. Dutta, C. Goulas, M. Steenbergen, R. Petrov, J. Sietsma, Design of high-strength and damage-resistant carbide-free fine bainitic steels for railway crossing applications, Mater. Sci. Eng. A 759 (2019) 210–223, doi: 10.1016/j.msea.2019.05.043.

[17] H.K.D.H. Bhadeshia, Bainite: overall transformation kinetics, J. Phys. 43 (1982) 443–448, doi: 10.1051/jphyscol:1982468.

[18] D. Quidort, Y. Bréchet, A model of isothermal and non isothermal transformation kinetics of bainite in 0.5% c steels, ISIJ Int. 42 (9) (2002) 1010–1017, doi: 10.2355/isijinternational.42.1010.

[19] D. Quidort, Y. Bréchet, The role of carbon on the kinetics of bainite transformation in steels, Scr. Mater. 47 (3) (2002) 151–156, doi: 10.1016/S1359-6462(02)00121-5.

[20] S.M.C. van Bohemen, Modeling start curves of bainite formation, Metall. Mater. Trans. A 41 (2) (2010) 285–296, doi: 10.1007/s11661-009-0106-9.

[21] C. Garcia-Mateo, F.G. Caballero, H.K.D.H. Bhadeshia, Acceleration of low-temperature bainite, ISIJ Int. 43 (11) (2003) 1821–1825, doi: 10.2355/isijinternational.43.1821.

[22] T. Sourmail, V. Smanio, Low temperature kinetics of bainite formation in high carbon steels, Acta Mater. 61 (7) (2013) 2639–2648, doi: 10.1016/j.actamat.2013.01.044.

[23] M. Umemoto, K. Horiuchi, I. Tamura, Transformation kinetics of bainite during isothermal holding and continuous cooling, Trans. ISIJ 22 (1982) 854–861, doi: 10.2355/isijinternational1966.22.854.

[24] S.-J. Lee, J.-S. Park, Y.-K. Lee, Effect of austenite grain size on the transformation kinetics of upper and lower bainite in a low-alloy steel, Scr. Mater. 59 (1) (2008) 87–90, doi: 10.1016/j.scriptamat.2008.02.036.

[25] F. Hu, P. Hodgson, K. Wu, Acceleration of the super bainite transformation through a coarse austenite grain size, Mater. Lett. 122 (2014) 240–243, doi: 10.1016/j.matlet.2014.02.051.

[26] G. Xu, F. Liu, L. Wang, H. Hu, A new approach to quantitative analysis of bainitic transformation in a superbainite steel, Scr. Mater. 68 (11) (2013) 833–836, doi: 10.1016/j.scriptamat.2013.01.033.

[27] H. Vetters, J. Dong, H. Bornas, F. Hoffmann, H.-W. Zoch, Microstructure and fatigue strength of the roller-bearing steel 100Cr6 (SAE 52100) after two-step bainitisation and combined bainitic-martensitic heat treatment, Int. J. Mater. Res. 97 (10) (2006) 1432–1440, doi: 10.3139/146.101388.Cited By 17

[28] A. Navarro-López, J. Sietsma, M.J. Santofimia, Effect of prior athermal martensite on the isothermal transformation kinetics below M_s in a low-C high-Si steel, Metall. Mater. Trans. A 47 (3) (2016) 1028–1039, doi: 10.1007/s11661-015-3285-6.

[29] H. Kawata, M. Takahashi, K. Hayashi, N. Sugiura, N. Yoshinaga, Effect of martensite in initial structure on bainite transformation, in: Proceedings of the THERMEC 2009, Materials Science Forum, 638, Trans Tech Publications, 2010, pp. 3307–3312, doi: 10.4028/www.scientific.net/MSF.638-642.3307.

[30] K. Zhu, H. Chen, J.-P. Masse, O. Bouaziz, G. Gachet, The effect of prior ferrite formation on bainite and martensite transformation kinetics in advanced high-strength steels, Acta Mater. 61 (16) (2013) 6025–6036, doi: 10.1016/j.actamat.2013.06.043.

[31] D. Quidort, Y. Bréchet, Isothermal growth kinetics of bainite in 0.5 steels, Acta Mater. 49 (20) (2001) 4161–4170, doi: 10.1016/S1359-6454(01)00316-0.

[32] A. Matsuzaki, H. Bhadeshia, Effect of austenite grain size and bainite morphology on overall kinetics of bainite transformation in steels, Mater. Sci. Technol. 15 (5) (1999) 518–522, doi: 10.1179/026708399101506210.

[33] M. Umemoto, T. Furuhara, I. Tamura, Effects of austenitizing temperature on the kinetics of bainite reaction at constant austenite grain size in Fe-C and Fe-Ni-C alloys, Acta Metall. 34 (11) (1986) 2235–2245, doi: 10.1016/0001-6160(86)90169-0.

[34] D. Raabe, M. Herbig, S. Sandlöbes, Y. Li, D. Tytko, M. Kuzmina, D. Ponge, P.-P. Choi, Grain boundary segregation engineering in metallic alloys: a pathway to the design of interfaces, Curr. Opin. Solid State Mater. Sci. 18 (4) (2014) 253–261, doi: 10.1016/j.cossms.2014.06.002.Slip Localization and Transfer in Deformation and Fatigue of Polycrystals

[35] Y. Li, D. Ponge, P. Choi, D. Raabe, Atomic scale investigation of non-equilibrium segregation of boron in a quenched mo-free martensitic steel, Ultramicroscopy 159 (2015) 240–247, doi: 10.1016/j.ultramic.2015.03.009.Part 2

[36] Y. Li, D. Ponge, P. Choi, D. Raabe, Segregation of boron at prior austenite grain boundaries in a quenched martensitic steel studied by atom probe tomography, Scr. Mater. 96 (2015) 13–16, doi: 10.1016/j.scriptamat.2014.09.031.

[37] M. Herbig, M. Kuzmina, C. Haase, R. Marceau, I. Gutierrez-Urrutia, D. Haley, D. Molodov, P. Choi, D. Raabe, Grain boundary segregation in fe-mn-c twinning-induced plasticity steels studied by correlative electron backscatter diffraction and atom probe tomography, Acta Mater. 83 (2015) 37–47, doi: 10.1016/j.actamat.2014.09.041.

[38] C. Cayron, ARPGE: A computer program to automatically reconstruct the parent grains from electron backscatter diffraction data, J. Appl. Crystallogr. 40 (6) (2007) 1183–1188, doi: 10.1107/S0021889807048777.

[39] K. Thompson, J. Sebastian, S. Gerstl, Observations of Si field evaporation, Ultramicroscopy 107 (2−3) (2007) 124–130, doi: 10.1016/j.ultramic.2006.06.007.

[40] S.K. Suram, K. Rajan, Calibration of reconstruction parameters in atom probe tomography using a single crystallographic orientation, Ultramicroscopy 132 (2013) 136–142, doi: 10.1016/j.ultramic.2013.02.013.{IFES} 2012

[41] Y. Xu, G. Xu, X. Mao, G. Zhao, S. Bao, Method to evaluate the kinetics of bainite transformation in low-temperature nanobainitic steel using thermal dilatation curve analys, Metals (Basel) 7 (330) (2017), doi: 10.3390/met7090330.

[42] B.W. Krakauer, D.N. Seidman, Absolute atomic-scale measurements of the gibbsian interfacial excess of solute at internal interfaces, Phys. Rev. B 48 (1993) 6724–6727, doi: 10.1103/PhysRevB.48.6724.

[43] M. Herbig, D. Raabe, Y.J. Li, P. Choi, S. Zaefferer, S. Goto, Atomic-scale quantification of grain boundary segregation in nanocrystalline material, Phys. Rev. Lett. 112 (2014) 126103, doi: 10.1103/PhysRevLett.112.126103.

[44] A.M. Ravi, J. Sietsma, M.J. Santofimia, Exploring bainite formation kinetics distinguishing grain-boundary and autocatalytic nucleation in high and low-si steels, Acta Mater. 105 (2016) 155–164, doi: 10.1016/j.actamat.2015.11.044.

[45] M.J. Santofimia, F.G. Caballero, C. Capdevila, C. Garcia-Mateo, C.G. de Andres, Evaluation of displacive models for bainite transformation kinetics in steels, Mater. Trans. 47 (6) (2006) 1492–1500, doi: 10.2320/matertrans.47.1492.

[46] M. Kang, M.-X. Zhang, F. Liu, M. Zhu, Kinetics and morphology of isothermal transformations at intermediate temperature in 15CrMnMoV steel, Mater. Trans. 50 (1) (2009) 123–129, doi: 10.2320/matertrans.MRA2008194.

[47] H. Farahani, W. Xu, S. van der Zwaag, Prediction and validation of the austenite phase fraction upon intercritical annealing of medium Mn steels, Metall. Mater. Trans. A 46 (11) (2015) 4978–4985, doi: 10.1007/s11661-015-3081-3.

[48] Z-Q. Liu, G. Miyamoto, Z-G. Yang, T. Furuhara, Direct measurement of carbon enrichment during austenite to ferrite transformation in hypoeutectoid fe-2mn-c alloys, Acta Mater. 61 (8) (2013) 3120–3129, doi: 10.1016/j.actamat.2013.02.003.

[49] T. Abe, K. Tsukada, H. Tagawa, I. Kozasu, Grain boundary segregation behaviour of phosphorus and carbon under equilibrium and non-equilibrium conditions in austenitic region of steels, ISIJ Int. 30 (6) (1990) 444–450, doi: 10.2355/isijinternational.30.444.

[50] M.K. Kang, Y.Q. Yang, Q.M. Wei, Q.M. Yang, X.K. Meng, On the prebainitic phenomenon in some alloys, Metallurgical and Materials Transactions A 25 (9) (1994) 1941–1946, doi: 10.1007/BF02649042.

[51] M.-X. Zhang, P. Kelly, Determination of carbon content in bainitic ferrite and carbon distribution in austenite by using CBKLDP, Mater. Charact. 40 (3) (1998) 159–168, doi: 10.1016/S1044-5803(98)00005-9.

[52] K. Tsuzaki, K. Fujiwara, T. Maki, Bainite reaction in Fe−Ni−C alloys, Mater. Trans., JIM 32 (8) (1991) 667–678, doi: 10.2320/matertrans1989.32.667.

[53] H. Aaronson, J. Hirth, On the thermodynamics of precipitate plate formation by shear above t0 assisted by solute adsorption effects, Scr. Metall. Mater. 33 (3) (1995) 347–353, doi: 10.1016/0956-716X(95)00222-H.

[54] H. Aaronson, G. Shiflet, Discussion to "determination of carbon content in bainitic ferrite and carbon distribution in austenite by using cbkld" by M.-X. Zhang and P. M. Kelly, materials characterization (1998) 40 159–168, Mater Charact. 54 (2) (2005) 177–181, doi: 10.1016/j.matchar.2004.08.008.

[55] P. Lejcek, Grain Boundary Segregation in Metals, Springer-Verlag Berlin Heidelberg, 2010, doi: 10.1007/978-3-642-12505-8.